

Fig. 39A-7-001.  $\text{Rb}_2\text{CoCl}_4$ .  $\kappa_a$  vs.  $T$  [88Shi].

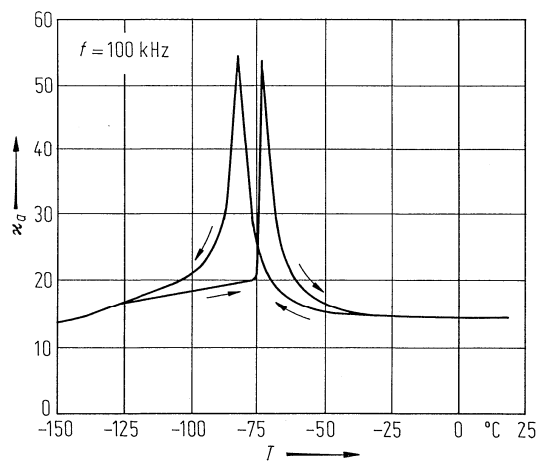


Fig. 39A-7-002.  $\text{Rb}_2\text{CoCl}_4$ .  $\kappa_a$  vs.  $T$  [88Shi].

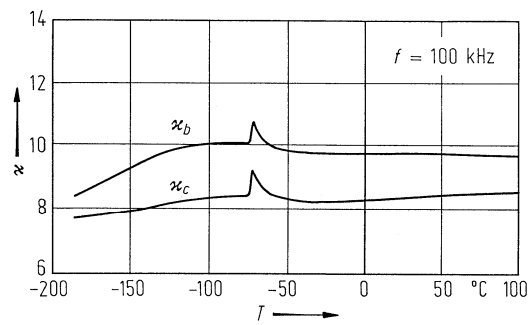
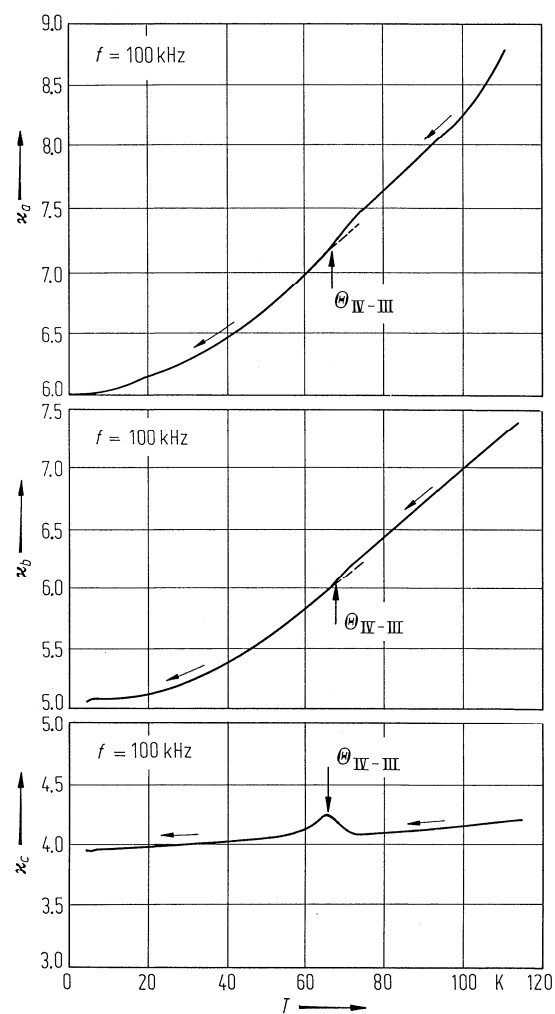
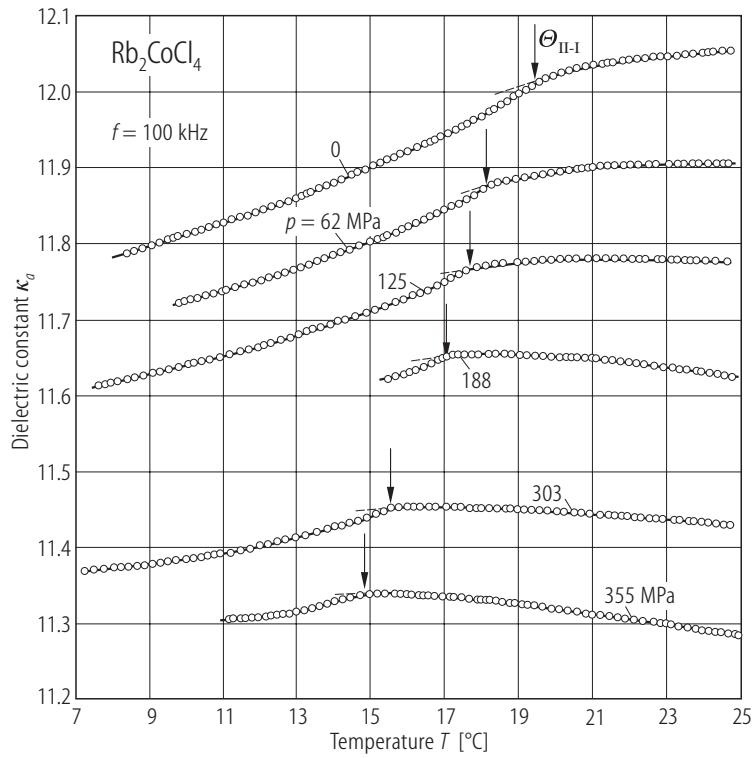


Fig. 39A-7-003.  $\text{Rb}_2\text{CoCl}_4$ .  $\kappa_b$ ,  $\kappa_c$  vs.  $T$  [88Shi].



**Fig. 39A-7-004.**  $\text{Rb}_2\text{CoCl}_4$ .  $\kappa_a$ ,  $\kappa_b$ ,  $\kappa_c$  vs.  $T$  around  $\Theta_{IV-III}$  [85Ges].



**Fig. 39A-7-005.**  $\text{Rb}_2\text{CoCl}_4$ .  $\kappa_a$  vs.  $T$  around  $\Theta_{\text{II-I}}$  [90Ges2]. Parameter:  $p$ .

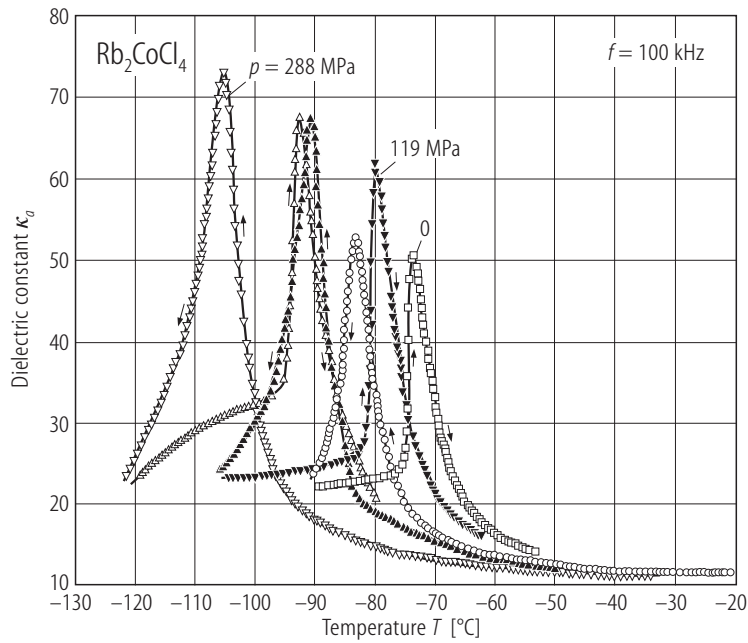


**Fig. 39A-7-006.**  $\text{Rb}_2\text{CoCl}_4$ .  $\kappa_a$  vs.  $T$  around  $\Theta_{\text{III-II}}$  [90Ges2]. Parameter:  $p$ .

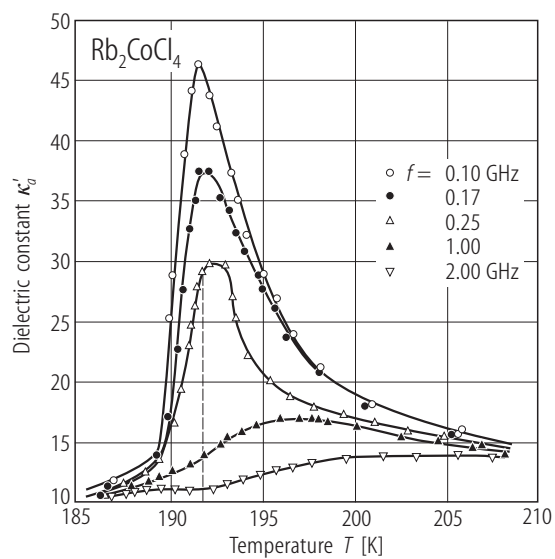


Fig. 39A-7-007.  $\text{Rb}_2\text{CoCl}_4$ .  $\kappa'_a$  vs.  $T$  [88Bre]. Parameter:  $f$ .

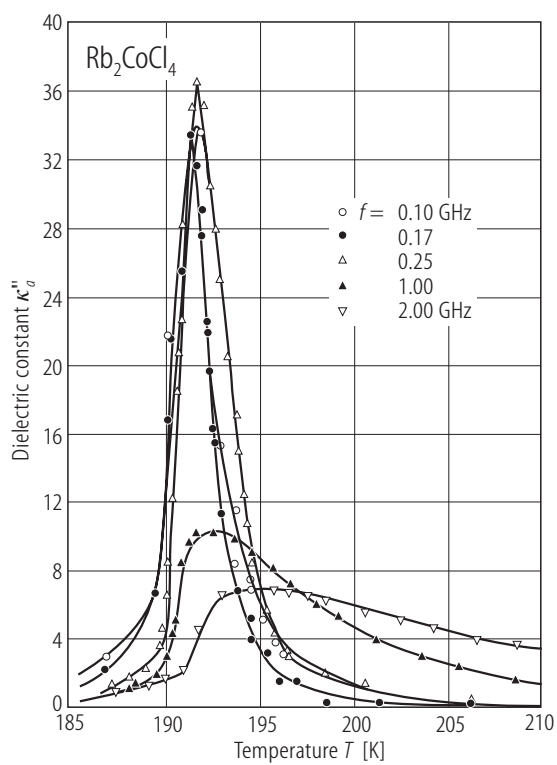
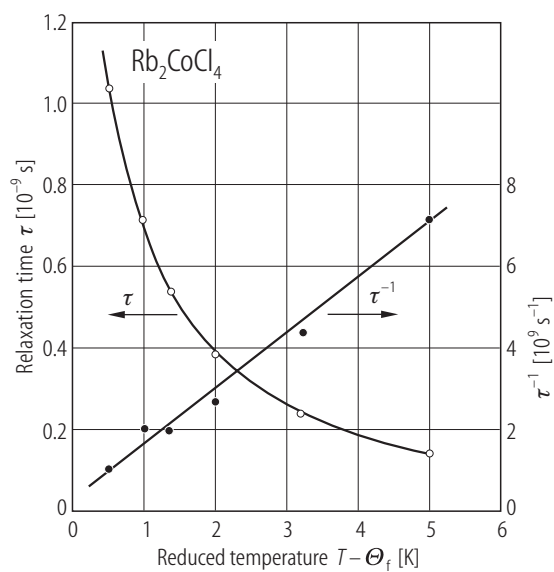
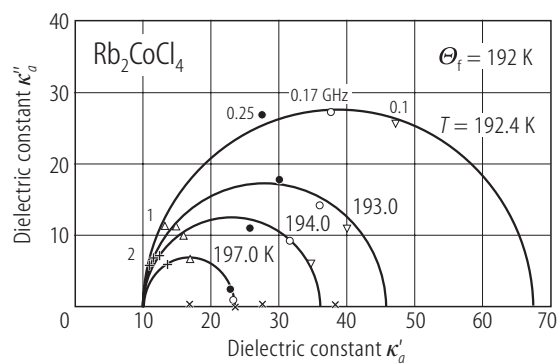


Fig. 39A-7-008.  $\text{Rb}_2\text{CoCl}_4$ .  $\kappa''_a$  vs.  $T$  [88Bre]. Parameter:  $p$ .  $f = 100$  kHz.



**Fig. 39A-7-009.**  $\text{Rb}_2\text{CoCl}_4$ .  $\tau$ ,  $1/\tau$  vs.  $T - \Theta_f$  [88Bre].  $\tau$ : dielectric dispersion time.



**Fig. 39A-7-010.**  $\text{Rb}_2\text{CoCl}_4$ . Cole-Cole plots of complex dielectric constant [88Bre]. Parameter:  $T$ . Cross: center of the Cole-Cole arc.

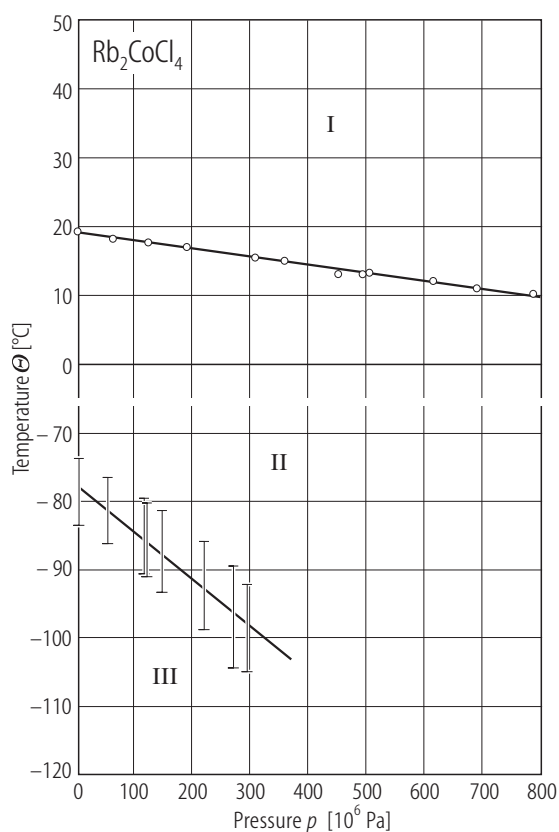


**Fig. 39A-7-011.** Rb<sub>2</sub>CoCl<sub>4</sub>.  $\Theta$  vs.  $p$  [90Ges2]. The vertical bars indicate the thermal hysteresis of the  $\Theta_{\text{II-III}}$ .

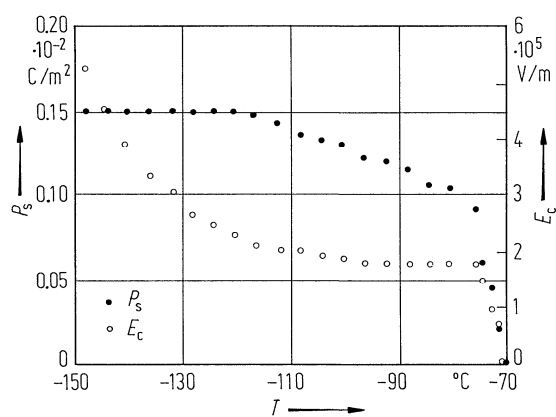


**Fig. 39A-7-012.** Rb<sub>2</sub>CoCl<sub>4</sub>.  $P_s$ ,  $E_c$  vs.  $T$  [88Shi].

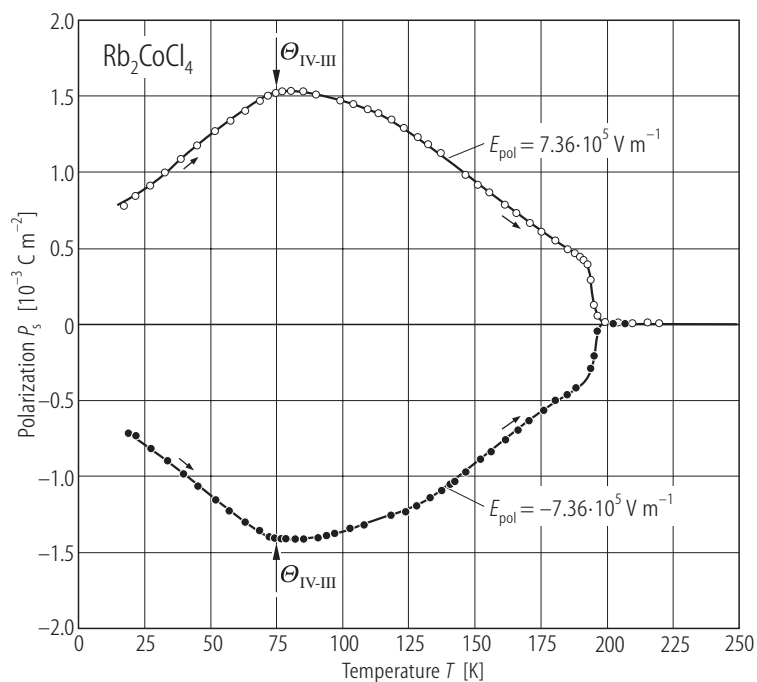


**Fig. 39A-7-013.** Rb<sub>2</sub>CoCl<sub>4</sub>.  $P_s$  vs.  $T$  [90Ges1].  $E_{pol}$ : poling field.

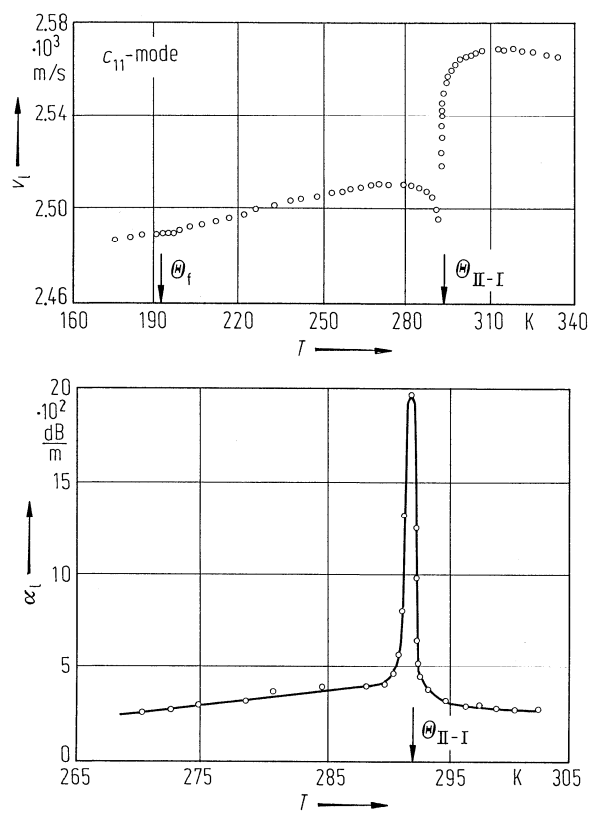


**Fig. 39A-7-014.** Rb<sub>2</sub>CoCl<sub>4</sub>.  $v_l$ ,  $\alpha_l$  vs.  $T$  [86Bre].  $v_l$ ,  $\alpha_l$ : sound velocity and attenuation of  $c_{11}$  mode.  $f=30$  MHz.

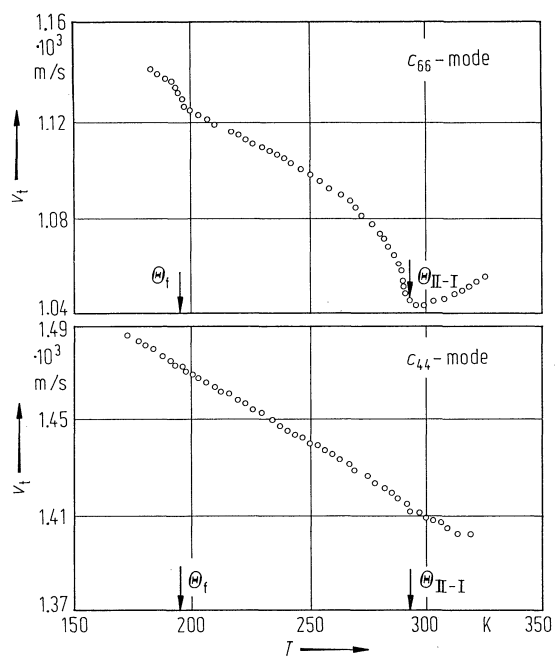


**Fig. 39A-7-015.** Rb<sub>2</sub>CoCl<sub>4</sub>.  $v_t$  vs.  $T$  [86Bre].  $v_t$ : sound velocities of transverse waves.  $f = 30$  MHz.

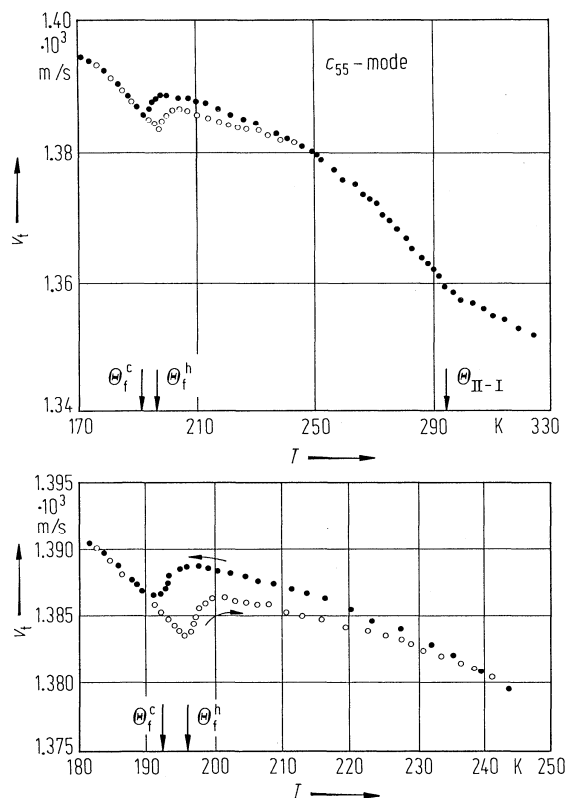


**Fig. 39A-7-016.** Rb<sub>2</sub>CoCl<sub>4</sub>.  $v_t$  vs.  $T$  [86Bre].  $v_t$ : sound velocity of  $c_{55}$  mode.  $f = 30$  MHz.  $\theta_f^c$  and  $\theta_f^h$  are  $\theta_{III-II}$  observed in cooling and heating runs, respectively.



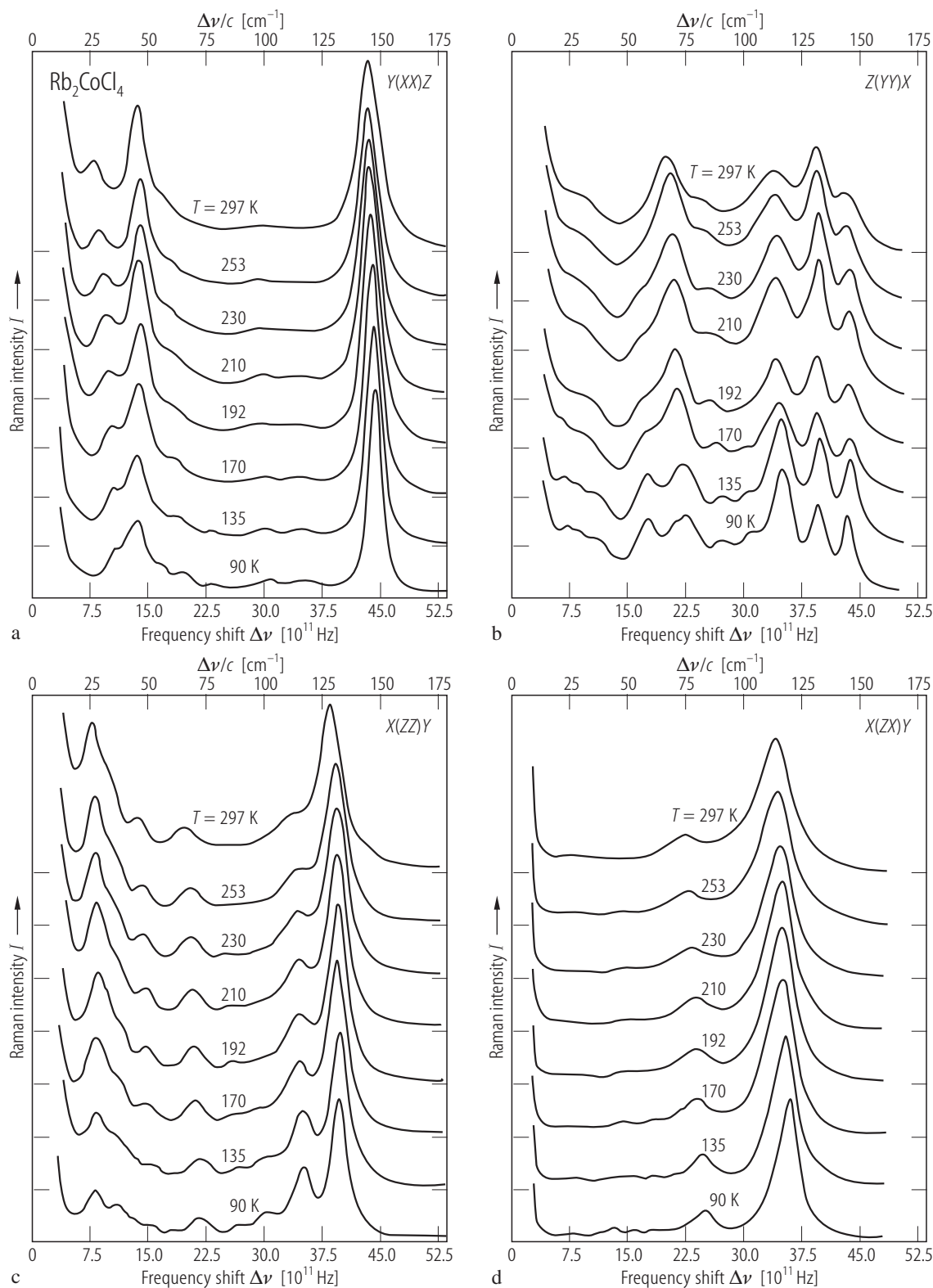


**Fig. 39A-7-017.**  $\text{Rb}_2\text{CoCl}_4$ .  $I$  vs.  $\Delta\nu$  [89Tor].  $I$ : Raman scattering intensity of (a)  $Y(XX)Z$ , (b)  $Z(Y\bar{Y})X$ , (c)  $X(ZZ)Y$ , (d)  $X(ZX)Y$  geometries. Parameter:  $T$ .

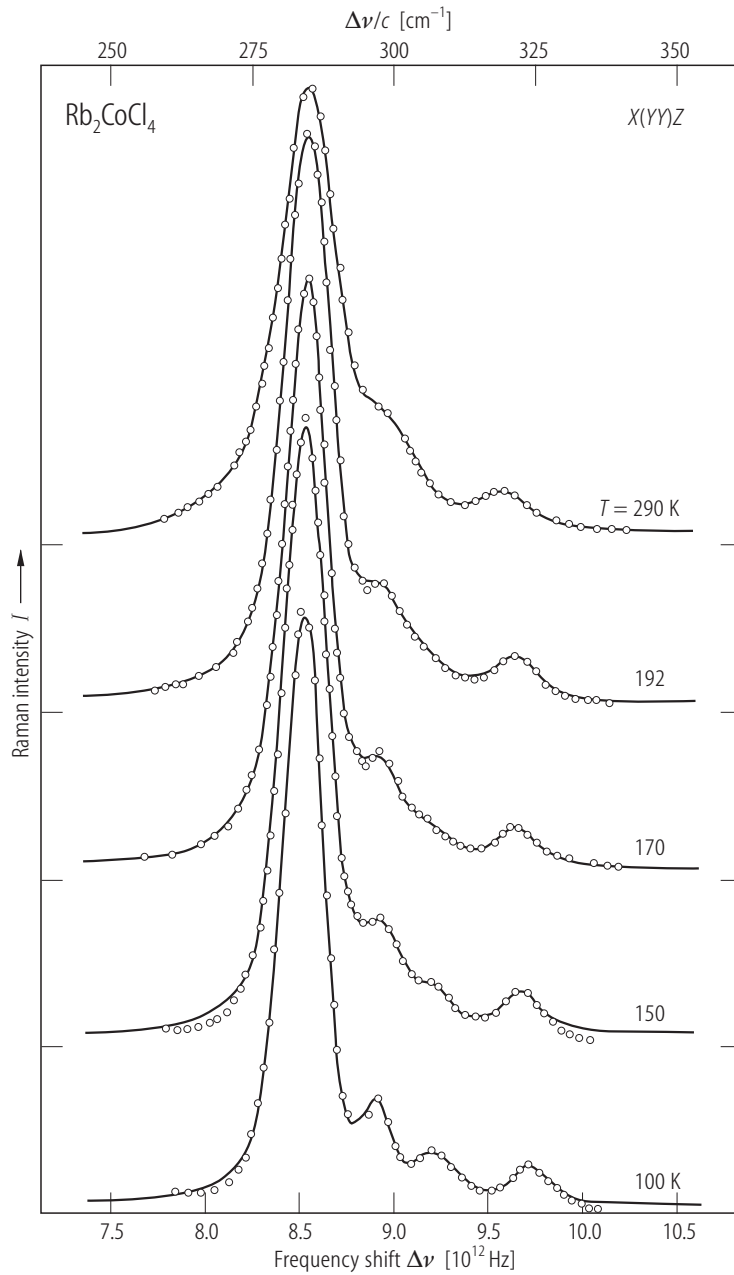


**Fig. 39A-7-018.**  $\text{Rb}_2\text{CoCl}_4$ .  $I$  vs.  $\Delta\nu$  [89Tor].  $I$ : Raman scattering intensity of the  $X(Y\bar{Y})Z$  geometry. Parameter:  $T$ .

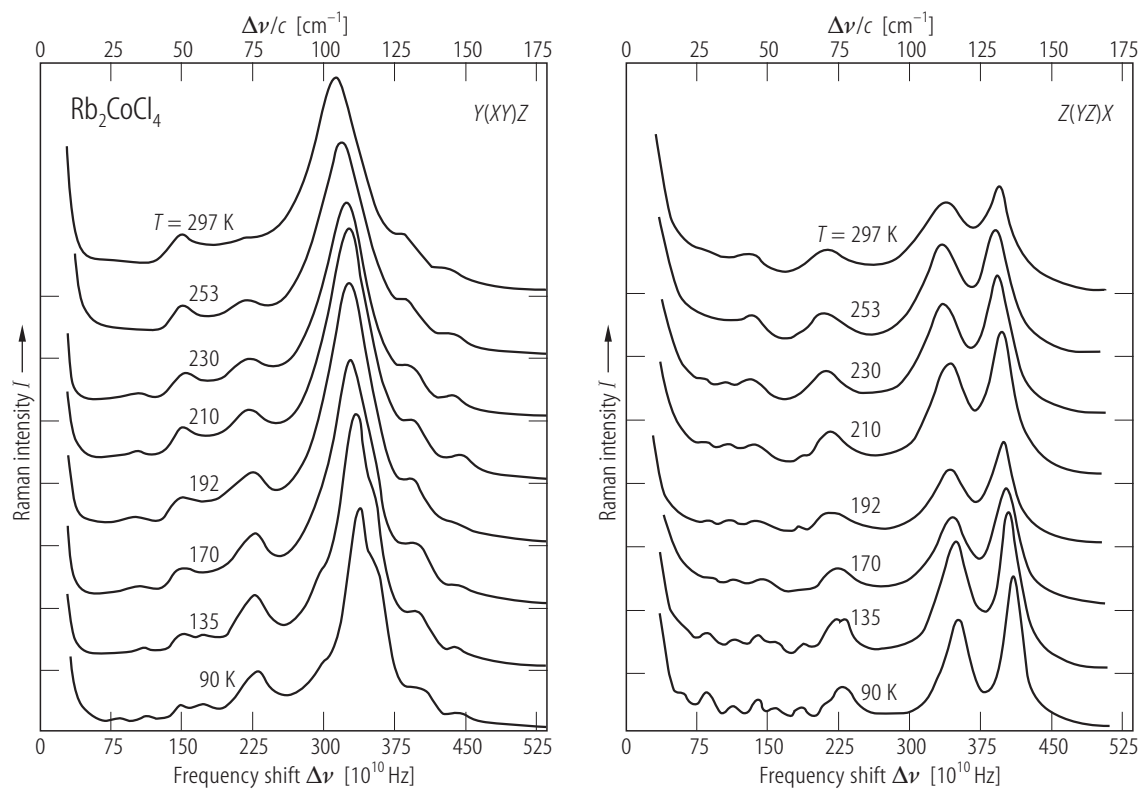


**Fig. 39A-7-019.**  $\text{Rb}_2\text{CoCl}_4$ .  $I$  vs.  $\Delta\nu$  [89Tor].  $I$ : Raman scattering intensity of the  $Y(XY)Z$  and  $Z(YZ)X$  geometries. Parameter:  $T$ .

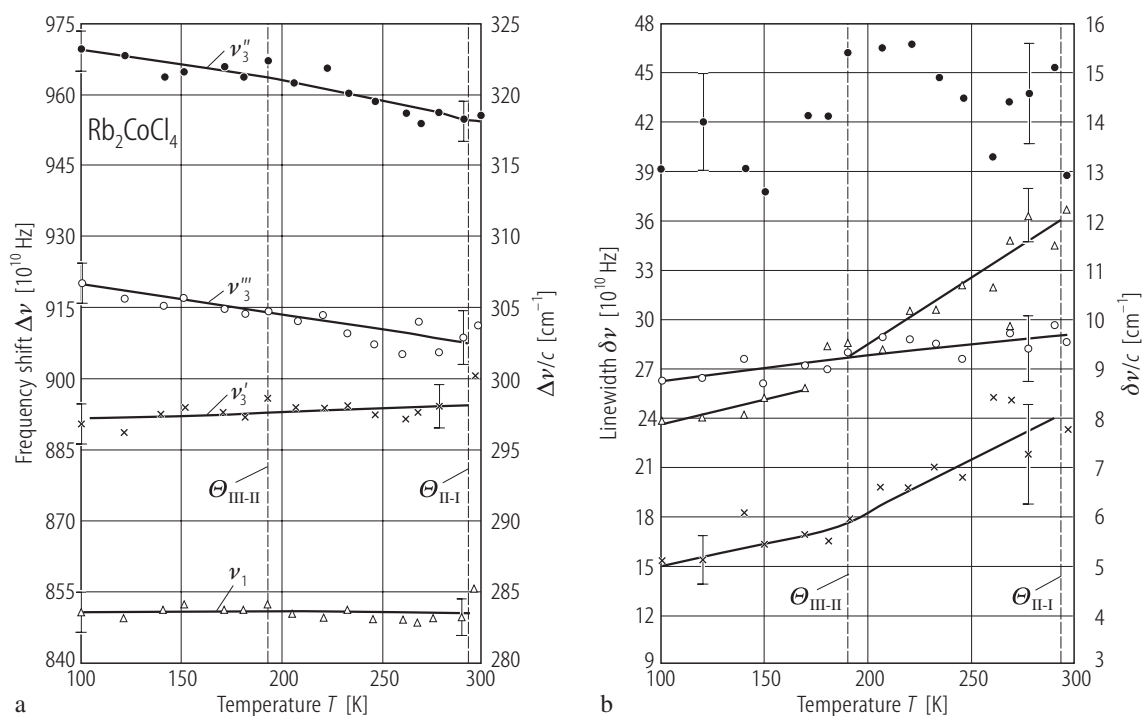


**Fig. 39A-7-020.** Rb<sub>2</sub>CoCl<sub>4</sub>. (a)  $\Delta\nu$  vs.  $T$ , (b)  $\delta\nu$  vs.  $T$  [89Tor].  $\Delta\nu$ : Raman scattering frequency shift,  $\delta\nu$ : linewidth of Raman line.

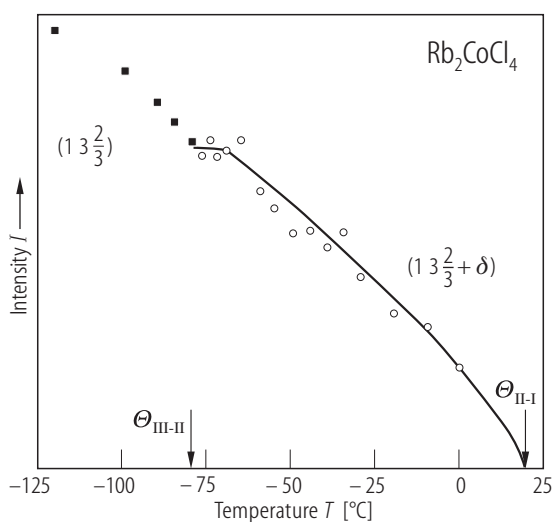


**Fig. 39A-7-021.** Rb<sub>2</sub>CoCl<sub>4</sub>.  $I$  vs.  $T$  [87Kas].  $I$ : integrated intensities of X-ray reflections at  $(1\ 3\ \frac{2}{3} + \delta)$ .

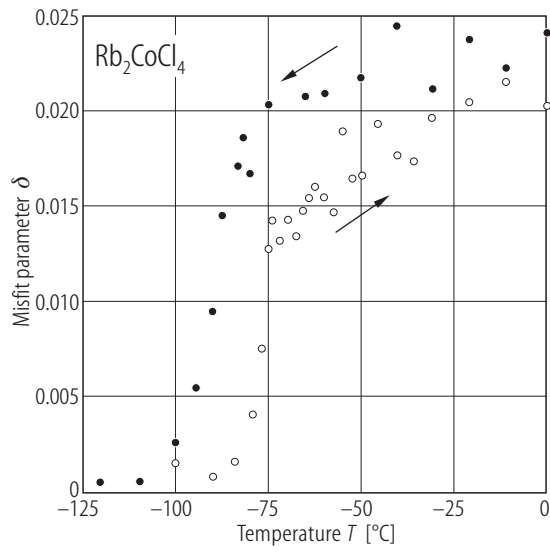


**Fig. 39A-7-022.**  $\text{Rb}_2\text{CoCl}_4$ .  $\delta$  vs.  $T$  [87Kas]. X-ray diffraction.  $\delta$  is defined by  $k_z = (1/3 - \delta) c_0^*$ , and  $c_0^*$  represents the reciprocal lattice constant in phase I.